

# Telescope Array Hybrid Composition and Auger-TA Composition Comparison

William Hanlon<sup>1,\*</sup> for the Telescope Array Project

<sup>1</sup>University of Utah Dept. of Physics and Astronomy & High Energy Astrophysics Institute, 201 James Fletcher Bldg., 115 S 1400 E, Salt Lake City, UT 84112, USA

**Abstract.** Telescope Array (TA) has completed analysis of nearly nine years of data measuring the atmospheric depth of air shower maximum ( $X_{\max}$ ) utilizing the TA surface detector array and the Black Rock Mesa and Long Ridge fluorescence detector stations. By using both the surface array and the fluorescence detector, the geometry and arrival time of air showers can be measured very precisely providing good resolution in determining  $X_{\max}$ .  $X_{\max}$  is directly related to the air shower primary particle mass and is therefore important for understanding the composition of ultra high energy cosmic rays (UHECRs). UHECR composition will help answer questions such as the distance and location of their sources. We discuss the experimental apparatus, analysis method, and  $X_{\max}$  data collected. We compare the energy dependent distributions of the observed data to detailed Monte Carlo simulations of four chemical species, then test which individual species are not compatible with the data through an analysis of the shapes of the distributions. We also discuss the present state of composition analysis and interpretation between the Auger and TA experiments. These are the two largest UHECR observatories in the world with large exposures and should shed light on UHECR composition.

## 1 Introduction

Ultra high energy cosmic ray (UHECR) mass composition remains a tantalizing source of inquiry even in the era of very large exposure detectors. Deeper understanding of the composition of UHECRs will shed light on which models of propagation and sources are viable. Because flux in the UHECR regime is low ( $J(E) \approx 3 \times 10^{-31} \text{ eV}^{-1} \text{ m}^{-2} \text{ s}^{-1} \text{ sr}^{-1}$ ) and is quickly falling with energy, composition cannot be directly measured on an event-by-event basis. Large detectors placed on the surface of the Earth, observing the resultant  $N_2$  fluorescence of air shower cascades produced by inelastic collisions of UHECR primaries and air are utilized instead. Observation of the depth of first interaction could be used to infer average primary particle mass given a large enough statistical sample, since this distribution is dependent upon the cross section with air which is related to particle mass. This method too is impractical due to the large distances between interaction depth and detector, low signal-to noise ratio, and relatively small detector acceptance. Air showers grow in size as a function of longitudinal depth, which is measured in  $\text{g/cm}^2$ , until the average energy per secondary particle falls below some critical energy. This depth is called  $X_{\max}$  and is observable out to several tens of kilometers by current fluorescence detectors (FDs) in use today [1, 2].

Given an ensemble of primaries of a single chemical element with varying energy, the mean  $X_{\max}$ ,  $\langle X_{\max} \rangle$ , in an energy bin is an increasing function of the logarithm of primary energy, called the elongation rate, and it is inversely proportional to the logarithm of the primary particle mass:

$\langle X_{\max} \rangle \propto D \ln(E/A)$ , where  $D$  is the elongation rate,  $E$  is the energy of the primary particle, and  $A$  is the mass number of the primary. Mixtures of primary elements have  $\langle X_{\max} \rangle \propto \langle \ln A \rangle$  [3, 4]. The width of a distribution of  $X_{\max}$ ,  $\sigma(X_{\max})$ , in an energy bin is also related to the primary particle mass. Intuitively we can guess this result if we consider a nucleus of mass number  $A$  and primary energy  $E$ , as a superposition of  $A$  nucleons with average energy  $E/A$ . This is reasonable in the limit of ultra high energies because the collision energy is much larger than the binding energy per nucleon. Hadronic induced showers are more complicated due to effects of elasticity and multiplicity, so  $\sigma(X_{\max})$  is larger than the naive approximation. For single elements it is found that  $\sigma(X_{\max})$  of the  $X_{\max}$  distribution in an energy bin decreases with increasing primary mass. For mixtures of elements  $\sigma(X_{\max})^2 \propto D^2(\langle \ln^2 A \rangle - \langle \ln A \rangle^2)$ , or  $\sigma(X_{\max})^2$  is proportional to the variance of  $\ln A$ . With these relations among  $\langle X_{\max} \rangle$  and  $\sigma(X_{\max})$ , we can simulate the UHECR flux arriving at a detector and compare the  $X_{\max}$  distributions,  $\langle X_{\max} \rangle$ , and  $\sigma(X_{\max})$  expected according to detector exposure to that observed in data. Hadronic air showers are complicated due to unknown parameters such as cross section, multiplicity, and elasticity for energies above those that can be recreated in the controlled experiments such colliders. Therefore hadronic models play an important role, and are an important contribution to systematic uncertainty, in understanding UHECR composition. Model uncertainties will be discussed further in section 2.

$X_{\max}$  is not observed by surface detectors (SDs), so, used alone, they cannot utilize the relationships discussed above to measure primary mass composition. Work is now

\*e-mail: whanlon@cosmic.utah.edu

progressing in TA and Auger through seeking to exploit the relationship between primary particle mass and the muon production in UHECR air showers [5, 6]. Muons produced in UHECR induced air showers are likely to survive to ground level and primaries of larger mass number produce more muons. This information can potentially be used to measure the primary mass composition on an event-by-event basis. One large advantage of this method is that SD arrays have 100% duty cycle and run continuously, while FDs run only on clear, moonless nights providing only a 10% duty cycle. Good sensitivity to muons and accurate hadronic models are required to do this. In particular it is now known that there are large discrepancies between model predictions of UHECR air shower muon flux on the ground and that predicted by the most recent hadronic models. TA and Auger each measure an excess of muons on the ground versus that predicted by QGSJet II and EPOS hadronic models [7, 8]. TA has measured  $\langle \ln A \rangle$  using nine years of SD data and a multivariate analysis technique up to  $E = 10^{20}$  eV, finding  $\langle \ln A \rangle = 1.52 \pm 0.08$  [6].

This paper will describe the most recent, highest statistics measurement of  $X_{\max}$  by Telescope Array in section 2. Section 3 will describe  $X_{\max}$  measurements of the two largest UHECR observatories and methods required to compare their results. Section 4 will summarize the details reported in this work.

## 2 Telescope Array $X_{\max}$ Results

Telescope Array is the largest cosmic ray observatory in the Northern Hemisphere, covering  $\sim 700$  km<sup>2</sup> in Millard County, Utah (39.3° N, 112.9° W, 1400 m asl). Placed within this area are 507 plastic scintillation surface detectors and three fluorescence detector stations. Each surface detector is 3 m<sup>2</sup> in area and holds two layers of plastic scintillator 1.25 cm thick. Each layer has 104 wavelength shifting fiber optic cables embedded in them, optically coupled to a PMT. Each SD contains FADC electronics modules to digitize signals from the PMTs, GPS modules to record times, and radio communications equipment to allow communication with one of three radio towers that monitor the SDs and runs regular diagnostics. When an SD records a low level trigger, which is simply some signal above threshold, they communicate this information to the radio towers which scan multiple low level triggers occurring nearly coincident in time. When the requirements for an event level trigger are met, the radio tower broadcasts for a readout of the neighboring SDs and stores the data for offline analysis [9].

The three FD stations are located to the north (Middle Drum), southwest (Long Ridge), and southeast (Black Rock) of the boundary of the SD array, each pointing towards the array center. The Middle Drum FD station employs 14 FD telescopes repurposed from the HiRes experiment [10]. The Black Rock (BR) and Long Ridge (LR) FD stations were newly constructed for the TA experiment. Each of these new FD stations utilize 12 telescopes, consisting of a 6.8m<sup>2</sup> mirror, focusing light onto a photomultiplier tube (PMT) cluster box containing 256 PMTs ar-

ranged in a 16x16 packed hexagonal array, and data acquisition (DAQ) hardware which includes FADC readout electronics, pattern recognition modules, and communications hardware to communicate with a central trigger distributor which directs readout and storage of data of all telescope DAQs when the condition for an event trigger is met [11, 12]. The twelve mirrors are arranged in a two ring configuration, with six mirrors in ring 1 observing between 3° - 18° in elevation, and six mirrors in ring 2 observing between 18° - 33°. Total azimuthal coverage is 108°.

$X_{\max}$  data is collected in hybrid mode by searching for time coincident events in the SD and FD data streams. Hybrid event observation allows for more accurate reconstruction of the shower track in the sky because it combines the FD observation of the shower along with the timing and geometry information of the SD. By using the SD timing and geometry, the shower angle ( $\psi$ ) in the shower-detector plane is very well constrained, allowing for a very accurate measurement of  $X_{\max}$ . Monocular reconstruction of showers has poor  $X_{\max}$  resolution compared to hybrid and stereo FD reconstruction methods. Multi-FD reconstruction of events also offers very good  $X_{\max}$  resolution, about the same as for hybrid reconstruction, but the acceptance of stereo events in TA is lower for  $E < 10^{19}$  eV due to the large distance between FD stations. Hybrid reconstruction provides the largest statistics study of  $X_{\max}$  in TA.

Previously TA has published results of hybrid  $X_{\max}$  using the Middle Drum FD station [13]. This present paper describes hybrid  $X_{\max}$  measurements utilizing the Black Rock and Long Ridge detectors. Black Rock and Long Ridge are “twins” using the same hardware, same electronics, and are similarly placed close to the border of the SD array (3 km and 4 km respectively), therefore they have similar hybrid acceptance. Middle Drum uses smaller mirrors and is placed about 8 km from the surface array border, giving it a very different acceptance particularly at low energies. Therefore Middle Drum reconstruction is not combined with Black Rock and Long Ridge events for this analysis.

This paper will summarize results of nearly nine years of BR/LR hybrid  $X_{\max}$  measurements recently published; further details about the analysis and results can be found there [14]. The data examined in this analysis spans the period 27 May 2008 to 29 November 2016, over which 1500 nights of data were collected. Time matching of BR/LR events and SD events resulted in 17,834 hybrid candidate events. An event only becomes an accepted hybrid event after it passes all quality cuts. Cuts on geometry such as track length cut, shower-detector plane cut, and zenith angle cut are used to ensure accurate reconstruction of the shower track. Cuts on fluorescence profile  $\chi^2$ ,  $X_{\max}$  bracketing, and good weather nights ensure the shower profile is well observed and  $X_{\max}$  is well measured. An energy cut is also applied to ensure that no events with reconstructed energy below  $10^{18.2}$  eV are accepted. This cut is imposed because of rapidly falling acceptance near this energy. After all quality cuts are applied 3330 events remain as accepted hybrid events for  $E \geq 10^{18.2}$  eV. To ensure the validity of our analysis TA makes extensive

use of a detailed Monte Carlo simulation which includes hourly and nightly databases of important runtime parameters such as PMT pedestals, PMT gains, mirror reflectivity, and atmospheric profile. We simulate the running conditions of each night's data that is collected to provide a simulated data sample approximately 10x that collected in data. Data and Monte Carlo are packed into the same data format and reconstructed using the same programs. Because of model dependencies and primary particle dependencies on observables, Monte Carlo is thrown for different models and primaries. In this work we compare TA  $X_{\max}$  data to QGSJet II-04 [15] protons, helium, nitrogen, and iron. We then perform data/Monte Carlo comparisons on observables that are important to good hybrid reconstruction of  $X_{\max}$ . Reconstruction bias and resolution is also checked by examining the difference between thrown and reconstructed values of important reconstruction parameters.  $X_{\max}$  reconstruction bias is -1.1, -3.3, -3.8, and -3.8  $\text{g/cm}^2$  for QGSJet II-04 protons, helium, nitrogen, and iron respectively for  $E \geq 10^{18.2}$  eV.  $X_{\max}$  resolution is 17.2  $\text{g/cm}^2$  for protons and 13.2  $\text{g/cm}^2$  for iron. Energy bias ranges from 1.7% for protons to -6.5% for iron, with energy resolution no worse than 6% for any of the four species examined. Resolution and bias of important geometric observables are very good as expected for hybrid reconstruction; angular resolutions are  $< 1^\circ$  and resolutions on  $R_p$  (shower impact parameter) and core location are  $\sim 50$  m.

We can compare the  $X_{\max}$  distributions of the data with that predicted by the Monte Carlo to see what elements best describe our observations. It is not clear what fraction of UHECRs in an energy bin are mixtures of different elements. For this work TA only compares data to the four individual QGSJet II-04 elements we simulated. This can be done by comparing the first two moments of the observed  $X_{\max}$  distributions in an energy bin, e.g.,  $\langle X_{\max} \rangle$  and  $\sigma(X_{\max})$ . Simplifying entire distributions to their first and second moments is problematic in the case of  $X_{\max}$  distributions though.  $X_{\max}$  distributions are not normal distributions and may exhibit significant skew depending upon the primary element being examined. Light elements such as protons and helium have large positive skew (right tail is longer), while heavy elements such as iron have a much less pronounced tail. This in and of itself may not be a problem when sufficient statistics are available in data. UHECR flux falls rapidly with energy though and appears to be cutting off above  $10^{19.7}$  eV [16]. This requires that UHECR observatories have very large exposures to provide sufficient statistics to generate a distribution of events that is not susceptible to statistical biases when measuring their means and widths. Hybrid reconstruction of  $X_{\max}$  is limited in its acceptance by requiring events fall within the boundaries of its SD array and TA's SD reconstruction is limited to zenith angles of  $60^\circ$ . These two constraints reduce the total acceptance of hybrid reconstructed events as energy increases because  $X_{\max}$  occurs closer to, or even in, the ground. Hybrid reconstruction of  $X_{\max}$  requires that  $X_{\max}$  be within the field of view of the FD ( $X_{\max}$  bracketing). As energy increases only tracks with increasing zenith angle have the potential to have sufficient

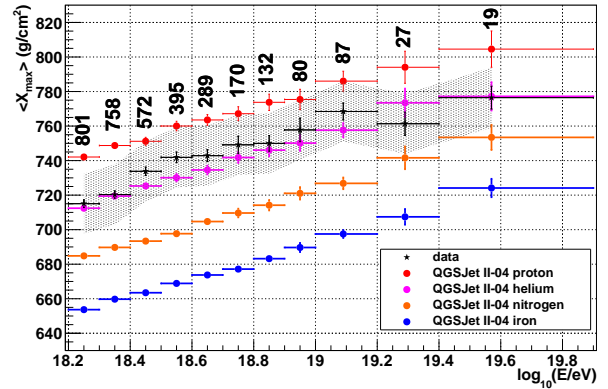


Figure 1: Mean  $X_{\max}$  as a function of energy as observed by Telescope Array in BR/LR hybrid mode over nearly nine years of data collection. The numbers above the data points indicate the number of events observed. The gray band is the systematic uncertainty of this analysis. Reconstructed Monte Carlo of four different primary species generated using the QGSJet II-04 hadronic model are shown for comparison.

track length to reach shower maximum in the atmosphere. Smaller zenith angle acceptance though reduces the FD field of view for showers that also arrive relatively close by due to the constraint imposed by the simultaneous SD detection as well. Standard FD-only observation has an aperture that grows with energy beyond the boundaries of the SD array, whereas hybrid can only grow up until the acceptance of the far side of the SD is fully efficient. TA SD reconstruction is currently limited up to zenith angles of  $60^\circ$  due to the difficulty of reconstructing the footprint of the shower at such large angles. Stereo FD reconstruction can address some of these problems. Stereo FD has equally good  $X_{\max}$  resolution as hybrid, is not limited to a smaller field of view at the highest energies, and has better acceptance than hybrid reconstruction at the highest energies. Because of the potential loss of the most deeply penetrating events at the highest energies, the potential for bias in  $\langle X_{\max} \rangle$  and  $\sigma(X_{\max})$  must be considered. We present the results of the first two moments of the observed  $X_{\max}$  distributions, but we also employ a morphological test of the shapes of the  $X_{\max}$  distributions and calculate the probability that a given element is compatible with our observations at the 95% confidence level.

Figure 1 and table 1 summarize the observed  $X_{\max}$  for nearly nine years of hybrid operations utilizing the BR and LR FD detectors in coincidence with the SD array. Figure 1 also shows the predicted  $\langle X_{\max} \rangle$  for the four QGSJet II-04 species simulated as well.  $\langle X_{\max} \rangle$  of the data differs greatly from nitrogen and iron, more closely resembling  $\langle X_{\max} \rangle$  of protons or helium. Notice that as energy increases the size of the energy bins must be increased to attempt to capture sufficient events to make a good measurement of  $\langle X_{\max} \rangle$  and  $\sigma(X_{\max})$ . Having only 27 or 19 events in a bin though, such as we have for  $E \geq 10^{19.2}$  eV, means we are susceptible to bias.

$E_{\text{low}}$	$\langle E \rangle$	$E_{\text{high}}$	$N_{\text{data}}$	$\langle X_{\text{max}} \rangle$	$\sigma(X_{\text{max}})$
18.20	18.25	18.30	801	$715 \pm 2^{+17}_{-17}$	$63 \pm 2^{+3}_{-4}$
18.30	18.35	18.40	758	$720 \pm 2^{+17}_{-17}$	$59 \pm 2^{+4}_{-4}$
18.40	18.45	18.50	572	$734 \pm 2^{+17}_{-17}$	$58 \pm 2^{+4}_{-4}$
18.50	18.55	18.60	395	$742 \pm 3^{+17}_{-17}$	$61 \pm 3^{+4}_{-4}$
18.60	18.65	18.70	289	$743 \pm 3^{+17}_{-17}$	$58 \pm 3^{+4}_{-4}$
18.70	18.75	18.80	170	$749 \pm 5^{+17}_{-17}$	$65 \pm 6^{+3}_{-4}$
18.80	18.85	18.90	132	$750 \pm 5^{+17}_{-17}$	$52 \pm 5^{+4}_{-4}$
18.90	18.95	19.00	80	$758 \pm 7^{+17}_{-17}$	$61 \pm 8^{+4}_{-4}$
19.00	19.09	19.20	87	$769 \pm 5^{+17}_{-17}$	$46 \pm 4^{+5}_{-5}$
19.20	19.29	19.40	27	$761 \pm 7^{+17}_{-17}$	$35 \pm 4^{+6}_{-7}$
19.40	19.57	19.90	19	$777 \pm 7^{+17}_{-17}$	$29 \pm 4^{+7}_{-9}$

Table 1:  $\langle X_{\text{max}} \rangle$  and  $\sigma(X_{\text{max}})$  observed for nearly 9 years of data by Telescope Array in BR/LR hybrid collection mode. Energy is in units of  $\log_{10}(E/\text{eV})$  and  $\langle X_{\text{max}} \rangle$  and  $\sigma(X_{\text{max}})$  are in  $\text{g}/\text{cm}^2$ .

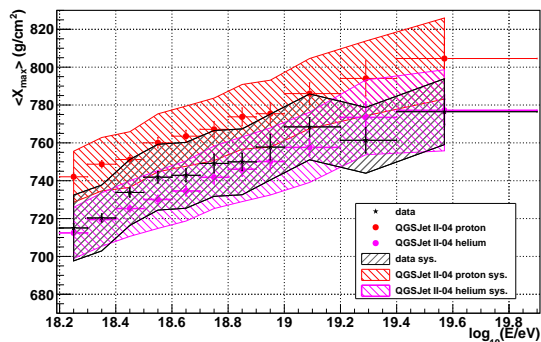


Figure 2: TA BR/LR observed hybrid  $\langle X_{\text{max}} \rangle$  and predictions for QGSJet II-04 protons and helium. The black band around the data is calculated systematic uncertainty of the data. The colored bands around the proton and helium predictions are estimated uncertainties in the QGSJet II-04 model.

We can measure the compatibility of the data with Monte Carlo by performing a maximum likelihood fit between their  $X_{\text{max}}$  distributions. To do this we need to address the potential of systematic uncertainties in our reconstruction and potentially in the models we are comparing against. We do this introducing a parameter  $\lambda$  by which we shift the data  $X_{\text{max}}$  distribution and finding the  $\lambda$  which gives the best likelihood between the data and Monte Carlo for a given energy bin and chemical element. The uncertainties in  $\langle X_{\text{max}} \rangle$  in hadronic models have been estimated to range from  $\sigma(\langle X_{\text{max}} \rangle) = \pm 3 \text{ g}/\text{cm}^2$  at  $10^{17.0} \text{ eV}$  to  $\sigma(\langle X_{\text{max}} \rangle) = \pm 18 \text{ g}/\text{cm}^2$  at  $10^{19.5} \text{ eV}$  [17]. Figure 2 shows the estimated systematic uncertainty in QGSJet II-04 protons and helium relative to TA  $\langle X_{\text{max}} \rangle$  and there is significant overlap between them. These uncertainties arise mainly from the relatively large unknown contributions from cross section, multiplicity, and elasticity in hadronic models that must be extrapolated from current collider energies up to the energies of UHECRs [18].

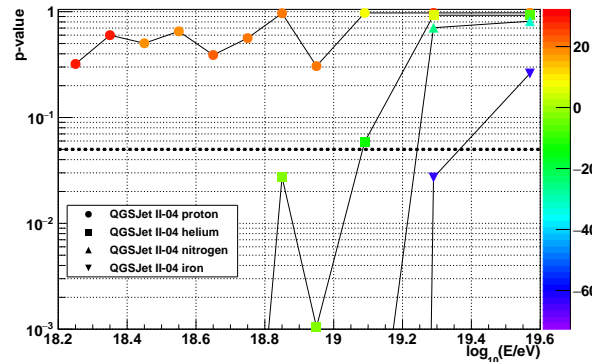


Figure 3: Unbinned maximum likelihood test on observed and simulated QGSJet II-04  $X_{\text{max}}$  distributions after systematic shifting of the data to find the best log likelihood. Each point represents the probability of measuring a log likelihood more extreme than that observed in the data after it is shifted by the best  $\Delta X_{\text{max}}$ . The color of the point indicates the  $\Delta X_{\text{max}}$  measured in  $\text{g}/\text{cm}^2$  required to find the maximum log likelihood value. The dashed line at  $p$ -value = 0.05 indicates the threshold below which the data is deemed incompatible with the Monte Carlo at the 95% confidence level.

We then calculate the chance probability of observing a likelihood at least as extreme as we find using the data. Using a critical value of 5%, we say that if the probability of observing a likelihood measured for the data and a given species is less than 5%, then the data is not compatible with the model at the 95% confidence level. If, on the other hand, the probability is greater than 5% we say that we cannot rule out that species as being the same as that which we have observed. We note that this is a simple test against single chemical elements, and does not test for compatibility for mixtures of elements. Our results do not preclude the possibility for mixtures of elements given that they occur in the correct ratios that would allow their distributions to mimic those we observe in our data. Figure 3 shows the results of these tests for QGSJet II-04 protons, helium, nitrogen, and iron. For all energies protons are found compatible with TA data. Helium does not become compatible with our data until  $E > 10^{19.2} \text{ eV}$ . Nitrogen becomes compatible for  $E > 10^{19.2} \text{ eV}$  and iron is compatible for  $E > 10^{19.4}$ . It may seem problematic that our  $X_{\text{max}}$  data is simultaneously compatible with  $X_{\text{max}}$  distributions whose shapes vary as widely as protons and iron at the highest energies. This reflects the lack of sufficient statistics to accurately measure the shapes of the distributions. In particular the tails of the distributions of the light elements disappear in these energy bins potentially because the  $X_{\text{max}}$  distribution is shifted deeper as it is approaching the limit of TA's reconstruction acceptance for such deeply penetrating events, even for simulated data. For iron though, figure 3 shows that the shift in  $X_{\text{max}}$  required to find the maximum likelihood requires a very large shift, approximately  $60 \text{ g}/\text{cm}^2$ , making it unlikely that iron is a truly reasonable match between the data and the Monte Carlo.

### 3 Comparison of Auger and Telescope Array $X_{\max}$

In the Southern Hemisphere, the Pierre Auger Observatory is the largest cosmic ray observatory currently in operation. It is located near Malargüe, Argentina. It uses 1660 water Cherenkov detectors covering 3000 km<sup>2</sup> and 24 fluorescence telescopes at four FD stations overlooking the SD array [19]. Auger also uses hybrid observation to measure  $X_{\max}$ .

Comparison of  $X_{\max}$  results between Auger and TA must account for the way each group analyzes their data. Auger reconstructs  $X_{\max}$  distributions as “seen in the atmosphere”, meaning they select events such that their final  $X_{\max}$  distributions for an energy bin are not biased by acceptance. This is done primarily through cuts on the field of view of the FD telescopes. For each energy bin, the upper and lower bound of the acceptable field of view is found by finding that range that does not allow true  $X_{\max}$  to deviate by more than 5 g/cm<sup>2</sup>. All observed showers must fall within this range otherwise it is not accepted. Other cuts are applied as well to ensure all events are high quality events. The effect of such a procedure is that the observed  $X_{\max}$  distributions will look like a distribution of simulated  $X_{\max}$  before it is distorted through acceptance of the detector [20]. Model dependence is still an issue and data must be compared to thrown models if one wishes to understand the distribution of chemical elements in the primary spectrum. Telescope Array reconstructs  $X_{\max}$  distributions as “seen by the detector”. TA imposes minimal cuts in an attempt to collect as many events as possible. In this approach, biases are incurred into a thrown  $X_{\max}$  distribution, caused by loss of events, e.g., high energy small zenith angle events that achieve shower maximum outside the field of view of the detector. This can have the effect of truncating tails in the reconstructed  $X_{\max}$  distributions and shifting their means and widths. We can still compare our data to simulations because we utilize a very detailed Monte Carlo simulation that informs us of our biases and distorts thrown distributions accordingly.

Even given this difference in approach to  $X_{\max}$  reconstruction, the data of TA and Auger do not look particularly different given each experiment’s uncertainties. Figure 4 shows the latest  $X_{\max}$  data collected by TA and Auger. Using nearly twelve years of data Auger has collected 10,570 events above  $E \geq 10^{18.2}$  eV compared to TA’s 3330 events [21]. Auger’s  $\langle X_{\max} \rangle$  is unbiased by the detector and TA’s  $\langle X_{\max} \rangle$  is biased. Without addressing this difference  $\langle X_{\max} \rangle$  cannot be compared in such a simple matter. Figure 4 also shows as reference the prediction each experiment makes for QGSJet II-04 protons. Auger’s  $\langle X_{\max} \rangle$  is consistent with their unbiased prediction with protons up to  $10^{18.7}$  eV, after which the data appears to signal an increase in primary mass. TA’s  $\langle X_{\max} \rangle$  is consistent with their prediction with protons within systematic uncertainties for  $E \geq 10^{18.5}$  eV. These results are often interpreted as Auger sees an evolution in composition to heavier primaries with energy, while TA sees composition compatible with light primaries such as protons.

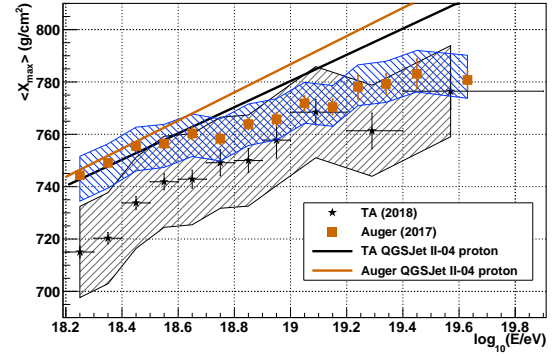


Figure 4: Most recent  $\langle X_{\max} \rangle$  measurements from TA (2018) [14] and Auger (2017) [21]. Systematic uncertainties for each measurement are indicated by the bands around the data points. The orange solid line and black solid line show each experiment’s prediction to compare against their data. Note that Auger’s proton prediction is unbiased by acceptance and reconstruction effects, while TA’s is biased.

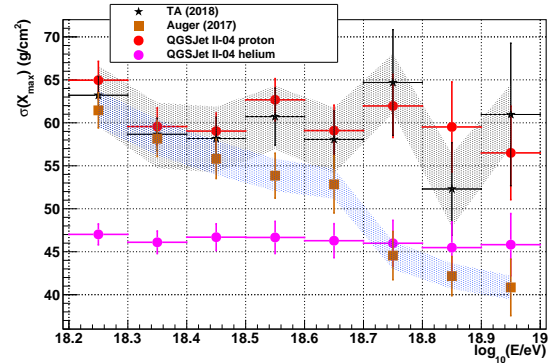


Figure 5: Most recent  $\sigma(X_{\max})$  measurements from TA (2018) [14] and Auger (2017) [21]. Systematic uncertainties for each measurement are indicated by the bands around the data points. The TA prediction for  $\sigma(X_{\max})$  of QGSJet II-04 protons and helium are also shown. Auger observes a narrowing of  $\sigma(X_{\max})$  for  $E \geq 10^{18.5}$  eV, while TA does not. Narrowing of  $\sigma(X_{\max})$  is signature of composition increasing in mass.

$\sigma(X_{\max})$  for each experiment also shows results consistent with these interpretations. Figure 5 shows recent measurements of  $\sigma(X_{\max})$  for both experiments. Below  $10^{18.5}$  eV Auger and TA observe the same  $\sigma(X_{\max})$ . Above this energy, Auger sees a narrowing of the  $X_{\max}$  distributions, which may be a sign of increasing primary particle mass.

Claims of disagreement between TA and Auger composition usually arise from naively interpreting the data as displayed in figures 4 and 5, without regard to the differences in TA and Auger reconstruction. To address the potential confusion arising from how to properly compare TA biased and Auger unbiased  $X_{\max}$  distributions, a Compo-



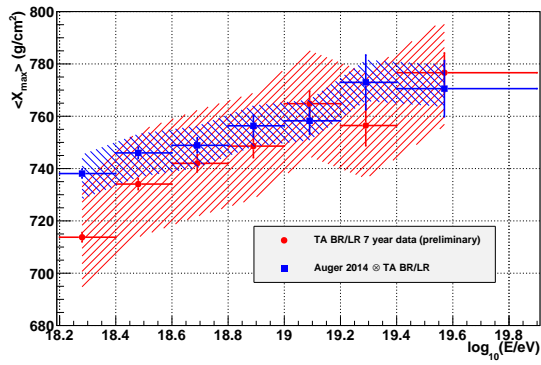


Figure 6: Comparison of Auger and TA  $X_{\max}$  measurements. TA data is that observed by the detector in the field. The Auger 2014  $\otimes$  TA BR/LR mixture is constructed by fitting Auger data to a mixture of four primary elements, throwing that energy dependent mixture in Monte Carlo, then reconstructing the mixture in the same way TA data is reconstructed. Within systematic uncertainties Auger and TA  $\langle X_{\max} \rangle$  are in agreement.

sition Working Group was formed in 2012 to allow  $X_{\max}$  analysis experts in each experiment to work together to determine the best way to make comparisons of each experiment's data [22]. In the years following, a procedure was developed to allow the direct comparison of Auger and TA data. The procedure is as follows: Auger fits their data to an ad-hoc mixture of proton, helium, nitrogen, and iron, computing the fractions of each as a function of energy, Auger provides these fractions to TA, TA performs a Monte Carlo simulation of the mixture, then compares the reconstructed mix to TA data. Because Auger's data is unbiased, a fit to their data is a fit to distributions generated by simulation without detector acceptance distorting them. By reconstructing that unbiased mixture through the TA analysis chain, and exposing the distributions to TA acceptance and reconstruction bias, this distorts the thrown distributions in a way that is consistent with how true distributions in nature are distorted.

The issue of which hadronic model best agrees with data must be addressed as well. Auger has fit its data to a few different models and finds best agreement with EPOS-LHC [23, 24]. In 2016, Auger and TA presented results of seven years of TA BR/LR hybrid  $X_{\max}$  data and a simulated mixture fit to Auger data and reconstructed through TA's analysis routines [25]. Figure 6 shows the result of employing the procedure previously described. Reconstruction of the mix that fits Auger data effectively biases it in the way the TA detector would see it. The figure shows that within systematic uncertainties Auger and TA are in good agreement in the measurement of  $\langle X_{\max} \rangle$ .

This analysis was extended further in 2017 [26]. In that study, the Auger mix was simulated by TA and reconstructed through TA analysis software, then the reconstructed  $X_{\max}$  distributions of the mixture were tested against the TA  $X_{\max}$  data distributions using both the Kolmogorov-Smirnov (KS) test and the Anderson-Darling

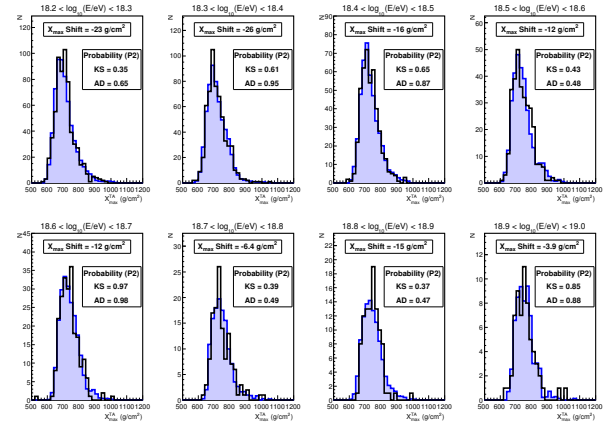


Figure 7: TA data  $X_{\max}$  distributions (black line) and Auger mix  $X_{\max}$  distributions (solid blue) used to test compatibility of TA and Auger data. TA data was allowed to be systematically shifted so that the means of the  $X_{\max}$  distributions matched. The KS and AD tests measure the probability of compatibility based upon the shapes of the distributions.

(AD) test. This procedure allowed us to test for compatibility of entire  $X_{\max}$  distributions, not just  $\langle X_{\max} \rangle$  and  $\sigma(X_{\max})$ , which is a more powerful and empirical measure. In each case the tests allow one to calculate the probability that both distributions were sampled from the same parent distribution. The KS test is most sensitive near the peak of distributions under test, while the AD test is more sensitive to the tails of the distributions [27]. Sensitivity to the tails is important for skewed distributions such as  $X_{\max}$ . To test the compatibility of the distributions, in an energy bin the Auger mix  $X_{\max}$  distribution reconstructed through the TA analysis chain was sampled according to TA data statistics, and the KS and AD test statistics were computed for this sample and the  $X_{\max}$  distribution of the mixture, called  $P1^{\text{MC}}$ . This was done 100,000 times and provides a distribution of probabilities for compatibility of the Auger mix in that energy bin. The probability that TA data and the Auger mix were sampled from the same distribution was also calculated and called  $P1^{\text{data}}$ . The compatibility probability of TA data and the Auger mix, P2, was then found by computing the probability to find  $P1^{\text{MC}}$  larger than  $P1^{\text{data}}$ . Because the Auger mix is generated using the Auger data, this provides a path for a direct measure of compatibility of Auger and TA  $X_{\max}$ .

Without systematic shifting of the TA data, only marginal compatibility was found between Auger and TA data. When TA  $X_{\max}$  distributions were allowed to vary systematically in an energy bin so that the means of the distributions matched, between 20 – 30 g/cm<sup>2</sup>, the compatibility probabilities indicated agreement for both two-sample tests. Figure 7 shows how the shapes of the TA and Auger mix distributions agree after shifting.

In addition, TA data was tested for compatibility with pure QGSJet II-04 protons and a similar level of agreement was found. Probabilities greater than 0.01 were considered compatible. The conclusion of the study was that, within

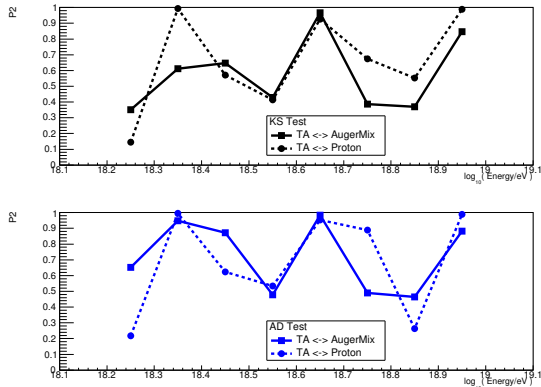


Figure 8: Compatibility probabilities ( $P_2$ ) between TA data and the Auger mix and QGSJet II-04 protons, using the Kolmogorov-Smirnov test (top) and Anderson-Darling test (bottom). Probabilities  $> 0.01$  indicate acceptable agreement between TA data and the distribution under test.

		Mix			Proton		
$E_{low}$	$E_{high}$	$\Delta$	KS	AD	$\Delta$	KS	AD
18.20	18.30	-23	0.35	0.65	-31	0.14	0.21
18.30	18.40	-26	0.61	0.95	-33	0.99	0.99
18.40	18.50	-16	0.65	0.87	-22	0.57	0.62
18.50	18.60	-12	0.43	0.48	-21	0.41	0.53
18.60	18.70	-12	0.97	0.98	-24	0.92	0.95
18.70	18.80	-6	0.39	0.49	-20	0.67	0.88
18.80	18.90	-15	0.37	0.47	-31	0.55	0.26
18.90	19.00	-4	0.85	0.88	-20	0.98	0.98

Table 2: Compatibility probabilities ( $P_2$ ) between Auger and TA data, and QGSJet II-04 protons and TA data using KS and AD two-sample tests.  $\Delta$  is shift in  $X_{max}$  in  $g/cm^2$  applied to the TA data.

systematic uncertainties, TA's and Auger's data are compatible, and TA data is also compatible, to about the same level, with a pure proton composition for  $E < 10^{19}$  eV. Work is continuing with the Composition Working Group to continue comparing data as both groups collect more data. Figure 8 shows the computed probabilities for all tests; table 2 summarizes the results.

## 4 Summary

Telescope Array has recently published the first results of UHECR  $X_{max}$  measurements for  $E \geq 10^{18.2}$  eV, using the Black Rock and Long Ridge FD stations in conjunction with the SD array. This nearly nine year hybrid data set is TA's highest statistics measure of  $X_{max}$ .  $\langle X_{max} \rangle$  and  $\sigma(X_{max})$  of the observed  $X_{max}$  distributions agree with a model consisting of light composition. Above  $10^{19}$  eV, statistics of TA's hybrid reconstruction begin to fall to levels that make testing data and Monte Carlo difficult. TA performed a test of compatibility of observed  $X_{max}$  with four different primary chemical elements using the QGSJet II-04 hadronic model. For each energy bin TA's

observed  $X_{max}$  distributions were allowed to shift systematically to find the shift which resulted in the largest maximum likelihood calculated between data and Monte Carlo. The chance probability of observing a likelihood at least as extreme as that found in the shifted data was computed for all four elements. Using this procedure it was found that TA data is compatible with QGSJet II-04 protons for all energies tested,  $10^{18.2} \leq E < 10^{19.9}$  eV. Helium is compatible for  $E \geq 10^{19}$  eV, nitrogen is compatible for  $E \geq 10^{19.2}$  eV, and iron is compatible for  $E \geq 10^{19.4}$  eV.

Auger and Telescope Array continue to work together through a Composition Working Group to allow the exchange of data and ideas to resolve the apparent discrepancies in the interpretation of UHECR composition. Auger and TA data cannot be directly compared because of the different approaches to analysis each experiment takes. Auger produces  $X_{max}$  distributions that are unbiased relative to true  $X_{max}$  distributions produced in UHECR simulations. TA produces  $X_{max}$  distributions which are biased due to detector acceptance and resolution. Because of these differences in analysis procedures, direct comparison of  $\langle X_{max} \rangle$  and  $\sigma(X_{max})$  does not provide an accurate picture of what the interpretation of UHECR composition should be. Instead, Auger and TA have developed a method of indirect comparison of data. Auger produces an energy dependent ad-hoc mixture of protons, helium, nitrogen, and iron that best fits their  $X_{max}$  distributions. This mixture is then simulated by TA and reconstructed in the normal manner. This causes the same biases to be applied to the data observed by TA. Tests of the reconstructed mix can then be performed to compare it to TA data. Work was done recently to test the compatibility probability of Auger and TA data using this procedure. It was found that TA data and Auger data are compatible between  $10^{18.2} \leq E < 10^{19.0}$  eV and the same level of compatibility was also found, using the same tests, between TA data and a pure proton composition. The Composition Working Group continues to work together to improve their understanding of each group's analysis and finding ways to compare their data.

## Acknowledgements

The Telescope Array experiment is supported by the Japan Society for the Promotion of Science (JSPS) through Grants-in-Aid for Priority Area 431, for Specially Promoted Research JP21000002, for Scientific Research (S) JP19104006, for Specially Promoted Research JP15H05693, for Scientific Research (S) JP15H05741 and for Young Scientists (A) JPH26707011; by the joint research program of the Institute for Cosmic Ray Research (ICRR), The University of Tokyo; by the U.S. National Science Foundation awards PHY-0601915, PHY-1404495, PHY-1404502, and PHY-1607727; by the National Research Foundation of Korea (2016R1A2B4014967, 2016R1A5A1013277, 2017K1A4A3015188, 2017R1A2A1A05071429); by the Russian Academy of Sciences, RFBR grant 16-02-00962a (INR), IISN project No. 4.4502.13, and Belgian Science Policy under IUAP VII/37 (ULB). The foundations of Dr.

Ezekiel R. and Edna Wattis Dumke, Willard L. Eccles, and George S. and Dolores Doré Eccles all helped with generous donations. The State of Utah supported the project through its Economic Development Board, and the University of Utah through the Office of the Vice President for Research. The experimental site became available through the cooperation of the Utah School and Institutional Trust Lands Administration (SITLA), U.S. Bureau of Land Management (BLM), and the U.S. Air Force. We appreciate the assistance of the State of Utah and Fillmore offices of the BLM in crafting the Plan of Development for the site. Patrick Shea assisted the collaboration with valuable advice on a variety of topics. The people and the officials of Millard County, Utah have been a source of steadfast and warm support for our work which we greatly appreciate. We are indebted to the Millard County Road Department for their efforts to maintain and clear the roads which get us to our sites. We gratefully acknowledge the contribution from the technical staffs of our home institutions. An allocation of computer time from the Center for High Performance Computing at the University of Utah is gratefully acknowledged.

## References

- [1] J.F. Carlson, J.R. Oppenheimer, *Phys. Rev.* **51**, 220 (1937)
- [2] J. Matthews, *Astropart. Phys.* **22**, 387 (2005)
- [3] R. Engel, D. Heck, T. Pierog, *Ann. Rev. Nucl. Part. Sci.* **61**, 467 (2011)
- [4] K.H. Kampert, M. Unger, *Astropart. Phys.* **35**, 660 (2012), 1201.0018
- [5] H. Wahlberg (Pierre Auger), *Nucl. Phys. Proc. Suppl.* **196**, 195 (2009)
- [6] R.U. Abbasi et al. (Telescope Array) (2018), 1808.03680
- [7] A. Aab et al. (Pierre Auger), *Phys. Rev. Lett.* **117**, 192001 (2016), 1610.08509
- [8] R.U. Abbasi et al. (Telescope Array), *Phys. Rev.* **D98**, 022002 (2018), 1804.03877
- [9] T. Abu-Zayyad et al. (Telescope Array), *Nucl. Instrum. Meth.* **A689**, 87 (2013), 1201.4964
- [10] T. Abu-Zayyad et al., *Nucl. Instrum. Meth.* **A450**, 253 (2000)
- [11] Y. Tameda et al., *Nucl. Instrum. Meth.* **A609**, 227 (2009)
- [12] H. Tokuno et al., *Nucl. Instrum. Meth.* **A676**, 54 (2012), 1201.0002
- [13] R.U. Abbasi et al., *Astropart. Phys.* **64**, 49 (2014), 1408.1726
- [14] R.U. Abbasi et al. (Telescope Array), *Astrophys. J.* **858**, 76 (2018), 1801.09784
- [15] S. Ostapchenko, *Phys. Rev.* **D83**, 014018 (2011), 1010.1869
- [16] T. Abu-Zayyad et al. (Telescope Array), *Astrophys. J.* **768**, L1 (2013), 1205.5067
- [17] R.U. Abbasi, G.B. Thomson (2016), 1605.05241
- [18] R. Ulrich, R. Engel, M. Unger, *Phys. Rev.* **D83**, 054026 (2011), 1010.4310
- [19] A. Aab et al. (Pierre Auger), *Nucl. Instrum. Meth.* **A798**, 172 (2015), 1502.01323
- [20] A. Aab et al. (Pierre Auger), *Phys. Rev.* **D90**, 122005 (2014), 1409.4809
- [21] J. Bellido (Pierre Auger), *PoS ICRC2017*, 506 (2018), [40(2017)]
- [22] E. Barcikowski, J. Bellido, J. Belz, Y. Egorov, S. Knurenko, V. de Souza, Y. Tameda, Y. Tsunesada, M. Unger (Yakutsk, Pierre Auger), *EPJ Web Conf.* **53**, 01006 (2013), 1306.4430
- [23] A. Aab et al. (Pierre Auger), *Phys. Rev.* **D90**, 122006 (2014), 1409.5083
- [24] T. Pierog, I. Karpenko, J.M. Katzy, E. Yatsenko, K. Werner, *Phys. Rev.* **C92**, 034906 (2015), 1306.0121
- [25] W. Hanlon, J. Bellido, J. Belz, S. Blaess, V. de Souza, D. Ikeda, P. Sokolsky, Y. Tsunesada, M. Unger, A. Yushkov, *JPS Conf. Proc.* **19**, 011013 (2018)
- [26] V. de Souza (Pierre Auger, Telescope Array), *PoS ICRC2017*, 522 (2018)
- [27] F.C. Porter (2008), 0804.0380